

Correcting systematic errors in the likelihood optimization of underdamped Langevin models of molecular dynamics trajectories

David Daniel Girardier,^{1, a)} Hadrien Vroylandt,² Sara Bonella,³ and Fabio Pietrucci¹

¹⁾ Sorbonne Université, Musée National d'Histoire Naturelle, UMR CNRS 7590, Institut de Minéralogie, de Physique des Matériaux et de Cosmochimie, IMPMC, F-75005 Paris, France

²⁾ Université Caen Normandie, ENSICAEN, CNRS, Normandie Univ, GREYC UMR 6072, F-14000 Caen, France

³⁾ Centre Européen de Calcul Atomique et Moléculaire (CECAM), Ecole Polytechnique Fédérale de Lausanne, Lausanne 1015, Switzerland

Since Kramers' pioneering work in 1940, significant efforts have been devoted to studying Langevin equations applied to physical and chemical reactions projected onto few collective variables, with particular focus on the inference of their parameters. While the inference for overdamped Langevin equations is well-established and widely applied, a notable gap remains in the literature for underdamped Langevin equations, which incorporate inertial effects and velocities. This gap arises from the challenge of accessing velocities solely through finite differences of positions, resulting in spurious correlations. In this letter, we propose an analytical correction for these correlations, specifically designed for a likelihood-maximization algorithm that exploits short, non-ergodic trajectories that can be obtained at reasonable numerical cost. The accuracy and robustness of our approach are tested across a benchmark case and a realistic system. This work paves the way for applying generalized Langevin equation inference to chemical reactions.

I. INTRODUCTION

In addition to providing ergodic canonical sampling for atomistic simulations of condensed phase systems, Langevin equations are often used to describe the time evolution of generic observables. As such, Langevin models have become everyday tools for a broad scientific community including applied mathematics, physics, chemistry, biology, and even finance. Indeed the flexibility of their structure, accommodating both deterministic and Markovian or non-Markovian random forces, enables them to model successfully phenomena as different as phase transitions¹, climate-change effects on ocean currents², and clocks³.

In particular, many complex, high-dimensional physical and chemical processes can be effectively studied through the lens of Langevin dynamics when projected onto one (or a few) collective variable (CV), q that tracks the progress of the transformation⁴. Depending on the problem, different types of Langevin equations should be adopted. In this work, we focus on the case of the underdamped, Markovian regime. In this case, the evolution equations are

$$\begin{cases} \dot{q} = v \\ \dot{v} = -\frac{1}{m} \frac{dF}{dq} - \gamma v + \tilde{\sigma} \eta(t) \end{cases} \quad (1)$$

where m is the effective CV mass, $F(q)$ the free energy landscape (or potential of mean force), $\gamma(q)$ is the friction, $\tilde{\sigma}$ is the amplitude of the random force, and $\eta(t)$ a time-uncorrelated Gaussian white noise. If

$\tilde{\sigma} = \sqrt{2 \frac{k_B T}{m} \gamma}$, fluctuation dissipation is enforced. In general, the potential of mean force and the friction are not available analytically and must be determined starting from observational time series of the CV and (in principle of) its velocity. These time series can come, for example, from experiments or atomistic molecular dynamics trajectories.

Furthermore, the stochastic equation is typically not employed in the differential form above, but rather translated into a numerical integrator with a finite time step⁵, τ , that establishes the time resolution adopted to analyze the data. Such resolution is a key parameter of the model: depending on the degree of temporal coarse-graining, different types of Langevin equations act as suitable approximations⁶. When an overdamped Langevin model is adequate, the parametrization of the dynamical system has been successfully achieved. For example, statistical inference approaches based on likelihood maximization allowed to reconstruct the potential of mean force, the diffusion coefficient (related to the friction) and the kinetic rate in a range of overdamped processes^{7–15}. We remark that long, ergodic trajectories that accurately sample the probability landscape of the CV are often unavailable, hence the importance to develop numerical schemes able to exploit also short, unbiased, non-ergodic trajectories¹⁵.

The parametrization of underdamped models is presently considerably less developed and understood. These models are, however, needed to describe important phenomena, such as migrating cells dynamics¹⁶ and biomolecular processes¹⁷, that display inertial effects at fine-grained time resolution, so progress in this direction is highly desirable. Unfortunately, model inference for the underdamped case is significantly more complex than for the overdamped. In the underdamped case,

^{a)} Electronic mail: david.girardier@sorbonne.universite.fr

CV positions and velocities appear on equal footings in Eq. 1. However, often in observational time-series only coordinates are directly accessible, while velocities need to be estimated via finite differences schemes¹⁸. This introduces spurious correlations even at infinitely-small time resolution, spoiling the accuracy of current inference methods.

In Ref.¹⁹, for example, it was shown that serious inaccuracies on friction estimation (subsequently affecting free energy estimation in non ergodic calculations), arise when the propagator deployed in the likelihood scheme is of order lower than $\mathcal{O}(\tau^{3/2})$. Unfortunately, no general solution for this problem was proposed. The spurious velocity correlations hinder also use of Kramers-Moyal expansion (see SI) or alternatives. For example, in Refs.^{17,20,21} only positions are employed in the parametrization of the potential of mean force and the friction (and diffusion) is obtained via local averages. This procedure, however, is based on an ad hoc choice of an integrator of first order in time and therefore open to the problems highlighted in Ref.¹⁹.

A solution to the problems arising from finite difference estimation of the velocities was proposed in Ref.¹⁶, where unbiased estimators for the drift and noise amplitude in Eq. 1 were derived. Even though this method represents a significant advance in the inference of realistic data, converging these estimators requires long simulations that might be unfeasible in the presence of free-energy barriers.

The approaches mentioned above are not based on likelihood maximization schemes. More recently, we proposed a likelihood-based scheme in which the velocity issue was circumvented by inferring the friction beforehand through correlation functions within a free-energy well⁶. This approach has the advantage of simplicity but it does not account for the position dependence of the friction and assumes that motion in one of the metastable states of the process can be approximated as harmonic.

In this letter, we propose a novel approach that overcomes the limitations of current inference schemes for underdamped Langevin models. Our method is based on likelihood maximization and only requires as input short, non ergodic trajectories, with velocities estimated from finite differences. An original analytical correction scheme eliminates nonphysical correlations from these estimates. We provide both a priori and a posteriori evaluations to the quality of the inference that do not require prior knowledge on the system. We demonstrate the accuracy and robustness of the approach with respect to varying the time resolution of the Langevin model across benchmark cases and realistic systems. In principle, the approach can be extended to non-Markovian generalized Langevin equations.

II. THEORY/METHODS

The projection of high-dimensional Hamiltonian dynamics onto one (or a few) CV(s) results in a generalized Langevin equation^{4,22}, that simplifies to the Markovian Eq. 1 for sufficiently coarse temporal subsampling⁶. Starting from a given set of trajectories discretized as M samples, an efficient strategy to parametrize Langevin models exploits the maximization of a likelihood function written as the product of short-time propagators:

$$\mathcal{L}_\theta = \prod_{n=1}^{M-1} \mathcal{P}_\theta(q_{n+1}, v_{n+1} | q_n, v_n) \quad (2)$$

where θ is the set of model parameter, which in our case include friction and free-energy landscapes. The mass is directly estimated using the equipartition theorem or via a coordinate transformation^{6,23}.

Following Refs.^{6,24} we approximate the propagator in Gaussian form

$$\begin{aligned} \mathcal{P}_\theta(q_{n+1}, v_{n+1} | q_n, v_n) = & \\ & \frac{1}{\sqrt{4\pi|M|}} \exp \left[-\frac{M_{qq}}{2|M|} (v_{n+1} - \langle v \rangle)^2 \right. \\ & \left. - \frac{M_{vv}}{2|M|} (q_{n+1} - \langle q \rangle)^2 + \frac{M_{qv}}{|M|} (q_{n+1} - \langle q \rangle)(v_{n+1} - \langle v \rangle) \right] \end{aligned} \quad (3)$$

where averages $\langle q \rangle, \langle v \rangle$ and (co)variances $M_{\alpha\beta} = \langle \alpha\beta \rangle - \langle \alpha \rangle \langle \beta \rangle$ (elements of the matrix M) are defined in SI section A.

As proved in SI section B, the specific form of the matrix and averages adopted in this work corresponds, to order $\mathcal{O}(\tau^3)$, to the evolution determined by the second order Vanden-Eijnden and Ciccotti (VEC) integrator for underdamped Langevin dynamics⁵:

$$q_{n+1} = q_n + \tau \left(1 - \frac{\gamma\tau}{2} \right) v_n + \frac{\tau^2}{2} \phi_n + \frac{\tau}{2} \sigma [G_n + \frac{1}{\sqrt{3}} \tilde{G}_n] \quad (4)$$

$$\begin{aligned} v_{n+1} = & \left(1 - \gamma\tau + \frac{\gamma^2\tau^2}{2} \right) v_n + \frac{\tau}{2} (\phi_n + \phi_{n+1}) + \sigma G_n \\ & - \gamma \frac{\tau^2}{2} \phi_n - \gamma \frac{\tau}{2} \sigma [G_n + \frac{1}{\sqrt{3}} \tilde{G}_n] \end{aligned} \quad (5)$$

with $\phi_n = -\frac{1}{m} \frac{dF(q_n)}{dq}$, $\sigma = \tilde{\sigma} \sqrt{\tau} = \sqrt{2 \frac{k_B T \gamma}{m} \tau}$, and G_n and \tilde{G}_n are two independent Gaussian white noises with unit variance. This correspondence can also be verified numerically. If exact positions and velocities of a VAC trajectory with integration time step τ are supplied to the likelihood expressions of Eqs. 2,3, the maximum value of Eq. 2 is obtained for the correct parameters of the underlying underdamped Langevin equation. This is illustrated in Fig. 1, that shows, for a double-well $F(q)$

landscape, different curves $-\log \mathcal{L}_\theta$ as a function of the friction. Let us focus, for the moment, on the dashed black curve in the figure, computed by feeding to the likelihood positions and velocities coming from a VEC trajectory: this curve has a minimum (and therefore the likelihood has a maximum) for $\gamma = 1$, which is, indeed, the friction used to integrate the trajectory.

In real applications, on the other hand, we need to estimate velocities starting from the observed positions at a given time resolution τ , resulting in a bias in the likelihood. This is illustrated via the purple curve in Fig. 1, that shows $-\log \mathcal{L}_\theta$ obtained using finite-difference velocities. We now describe how this problem can be efficiently and accurately corrected. Let us consider the time-reversible¹⁶ central finite difference estimator of the velocity $u_n = \frac{q_{n+1} - q_{n-1}}{2\tau}$, combined with the VEC integrator. In SI section C, it is shown that, up to order $\tau^{3/2}$, the difference between u_n and the integration velocity v_n is given by:

$$v_n = u_n - \frac{\sigma}{4} \left[G_n + \frac{1}{\sqrt{3}} \tilde{G}_n - G_{n-1} + \frac{1}{\sqrt{3}} \tilde{G}_{n-1} \right] + \mathcal{O}(\tau^{3/2}) \quad (6)$$

Using this result, the properties of Gaussian white noises and their correlations with positions or velocities as described in SI section D, we can recover the correct values for averages appearing in the likelihood:

$$\langle v_n^2 \rangle = \langle u_n^2 \rangle + \frac{\sigma^2}{3} + \mathcal{O}(\tau^{3/2}) \quad (7)$$

$$\langle v_n v_{n-1} \rangle = \langle u_n u_{n-1} \rangle + \frac{\sigma^2}{24} + \mathcal{O}(\tau^{3/2}) \quad (8)$$

$$\langle v_n q_n \rangle = \langle u_n q_n \rangle + \mathcal{O}(\tau^{3/2}) \quad (9)$$

$$\langle v_n q_{n+1} \rangle = \langle u_n q_{n+1} \rangle + \mathcal{O}(\tau^{3/2}) \quad (10)$$

$$\langle v_{n+1} q_n \rangle = \langle u_{n+1} q_n \rangle \quad (11)$$

These corrected averages enable to remove from the log-likelihood the spurious correlations that lead to substantial systematic errors for inferred free-energy and friction landscapes can be prevented. Note that the corrections depend implicitly on the friction γ , one of the parameters that must be inferred, via σ . We then propose the following expectation-maximization scheme:

1. likelihood optimization without correction
2. correction of the likelihood with the previously obtained friction and new optimization
3. repetition until convergence

The efficiency of the iterative scheme is demonstrated in Fig. 1, where, after 5 iterations, the correction added to finite difference velocity likelihood (dark-red curve) allows to recover the likelihood computed using the integration velocity (dashed curve).

As a first full illustration of the validity and efficiency of the new algorithm, we infer the parameters of the

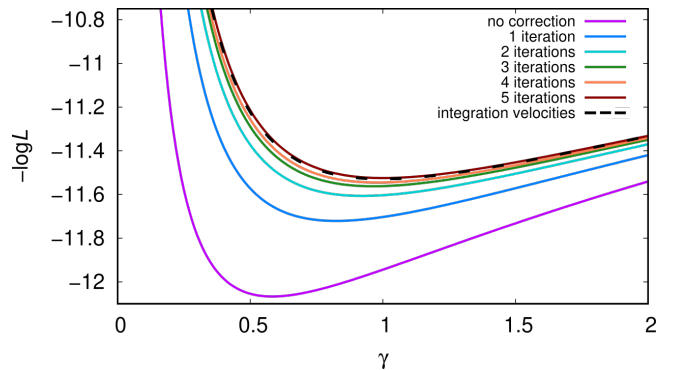


FIG. 1. Corrected log-likelihood estimated from the finite-difference velocity using Eqs. 7,8, as a function of the friction γ , for non-ergodic trajectories of a double-well system (with free energy and mass fixed to their optimal values), for different numbers of iterations of the correcting scheme. The non-corrected curve is displayed for comparison. The dashed line represents the log-likelihood computed from the integration velocities.

underdamped Langevin equation from one-dimensional generalized Langevin trajectories in a double-well landscape (Fig. 2). The goal is to mimic a typical application, where high-dimensional MD trajectories are projected on a collective variable, leading to non-Markovian behavior that is captured by the generalized Langevin equation⁶ (see SI section F). Furthermore, we consider relatively-short non-ergodic trajectories (Fig. 2a), since in realistic barrier-crossing processes it is unfeasible to perform ergodic MD simulations.

In order to determine whether the initial data can be accurately reproduced with an underdamped Langevin model, there are two characteristic timescales that define the lower and upper bounds for inference. The lower bound is set by the decay time of the memory kernel and the upper bound is determined by the velocity decorrelation time. τ has to be coarse-enough to lose non-Markovian effects, while providing sufficient resolution to capture the original velocity autocorrelation function (VACF). The dashed black curve in Fig. 2c shows that, for our double well system, a time resolution τ in the range 0.01–0.02 ps defines the optimal regime for underdamped inference.

Our iterative correction scheme is then applied to data for which the velocity can only be accessed through finite differences. This arises from the temporal subsampling applied to the data to avoid memory effects, which leaves only the positions accessible. We then systematically compare the statistical properties of original trajectories with those of the underdamped models generated at different τ values. The sampling trajectories and results for the inferred free energy and friction are presented in the different panels of Fig. 2. First, the free-energy landscape is accurately reproduced up to $\tau = 0.02$ ps (including for τ shorter than the memory kernel decay, surprisingly), while an error larger than $k_B T$ appears at $\tau = 0.1$ ps.

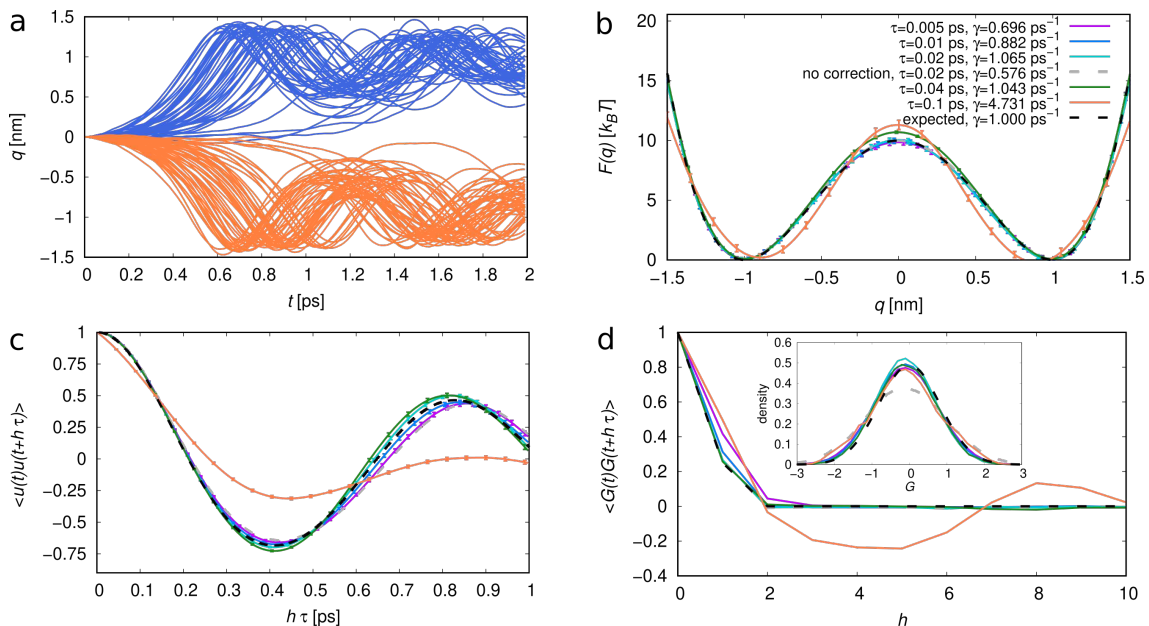


FIG. 2. Benchmark system for the new inference approach. (a) non-Markovian Langevin trajectories relaxing from the top of a barrier, integrated with a 0.1 fs time step and unit mass. The memory kernel is $K(t) = 500 \exp(-t/0.002) \text{ ps}^{-2}$, with an integral yielding unitary friction. (b) Free-energy profiles and friction coefficients for underdamped models inferred at different time resolutions τ with the likelihood correction (except the dashed gray curve, for comparison). (c) Velocity autocorrelation function of the original trajectories and of synthetic ones generated from the models using the Euler–Maruyama integrator. (d) Correlation analysis of the noise time series deduced from the trajectories in panel (a) by inverting the positional part of Vanden-Eijnden Ciccotti integrator. The inset shows the noise distribution.

Likewise, the errors on the inferred friction coefficient, on the VACF and on the noise autocorrelation function become unacceptable at the largest τ , with acceptable accuracy for finer time resolutions (Fig. 2). We remark that the time correlation of the noise recovered from the original trajectories and inferred models is particularly insightful and can be used to provide a further diagnostic tool for the accuracy of the inference. Its analytical behaviour is in fact known (see SI section G).

In summary, all diagnostics indicate that the most accurate models are obtained for τ in the range 0.01–0.02 ps, even though the error is moderate for $\tau = 0.005$ or 0.04 ps. It is important to note that, without applying the correction scheme, the model is inaccurate even for an optimal choice of τ (0.02 ps). In this case, the friction is the most significantly affected parameter, with only approximately $\sim 2/3$ of its original value (compatible with Ref.¹⁹).

We now focus on a realistic physical system, formed by two C_{60} fullerene nanoparticles immersed in liquid water, modeled as a periodically-repeated cubic simulation box including 2398 water molecules (Fig. 3a). We perform MD simulations at 300 K in the NVT ensemble²⁵, with a timestep of 1 fs, as implemented in GRO-MACS 2019.4 code²⁶, with the SPC water force field²⁷ and OPLS-AA²⁸ for carbon. For computational details we refer to Ref.⁶. We modified the masses of oxygen and carbon to 1 and 120 a.u., respectively: without affecting the free-energy landscape, this ensures a wider range of

time resolutions for the accurate reconstruction of underdamped models (see SI section I for comparisons with unmodified masses).

We analyze the dissociation/association process of the fullerene dimer, employing 500 short (40 ps) unbiased MD trajectories relaxing from the transition state ensemble, generated with the aimless shooting algorithm^{15,29}. The high-dimensional trajectories are projected onto one CV, defined as the distance between the centers of mass of the two fullerenes (Fig. 3b). Albeit sub-optimal, this CV is able to capture the main features of the transition process: in particular, explicitly including water degrees of freedom does not improve the kinetic description³⁰.

As for the benchmark case, as a first step we determine a time resolution τ that avoids memory effects while maintaining smoothness in the VACF. The memory kernel in Fig. 3c, computed using the Volterra method of Ref.³¹ on a locally-equilibrated 10 ns trajectory of the dimer, indicates that $\tau \geq 0.1$ ps is required to eliminate most non-Markovian effects, notwithstanding a surviving tail in the memory kernel. We make here the customary approximation of a position-independent kernel.

To ensure a good representation of the VACF (Fig. 4c, dashed line), the upper bound is set as $\tau < 1.0$ ps. Thus, we conclude that the inference of underdamped Langevin models can be attempted for $0.1 \leq \tau < 1.0$ ps. We apply our inference scheme in this range, obtaining the free-energy profile and the position-dependent friction by likelihood maximization, while estimating the mass via

equipartition of kinetic energy.

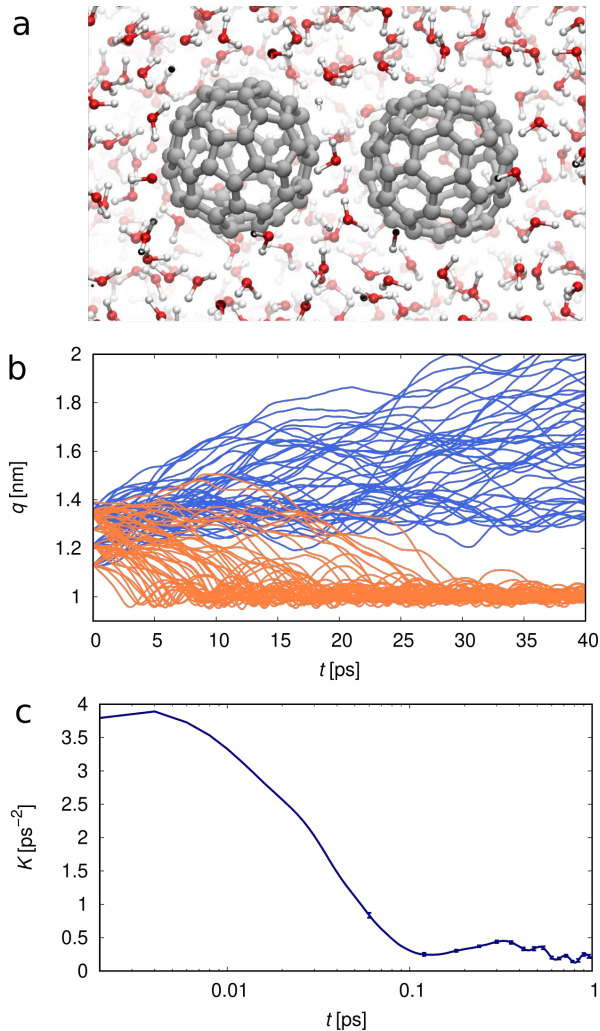


FIG. 3. (a) Atomistic representation of the C₆₀ dimer in water solution. (b) Aimless shooting trajectories projected onto the distance between the C₆₀ centers of mass. (c) Memory kernel computed for the associated state of the dimer, using the Volterra method in Ref.³¹.

As a first observation, we note that the inferred free-energy profiles are in good agreement with the brute-force reference, particularly in the dimer region, except for the largest time resolution $\tau = 1$ ps. For $0.1 \leq \tau \leq 0.5$ ps, the barrier height is consistent within $1 k_B T$ across models, even though the transition-state region is best captured by the $\tau = 0.5$ ps model. We emphasize again the importance of the correction, that here has a strong effect on the free energy barrier (*vide infra*).

Indeed, comparison of the VACF for the different models with the one from the original MD simulation (Fig. 4b) confirms that the time resolution $\tau = 0.5$ ps is the most suitable for accurately modeling the projected dynamics.

Finally, the same resolution appears optimal also by

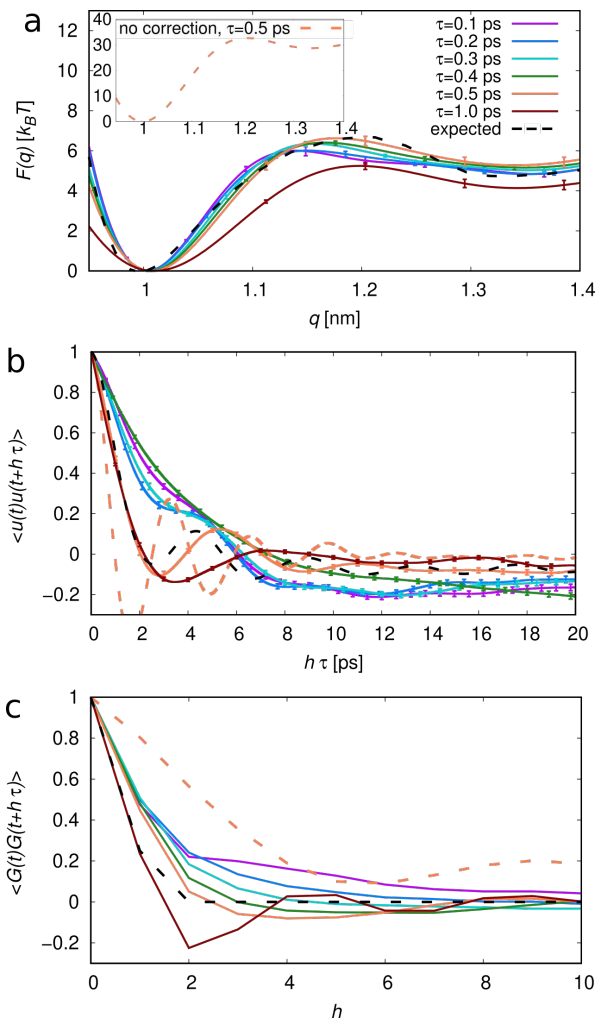


FIG. 4. Properties of underdamped Langevin models of fullerene dimer dynamics parametrized from aimless shooting trajectories. (a) Free-energy profiles at different time resolutions τ using the likelihood correction (the dashed orange curve shows the result without correction, for comparison, with a $\approx 30 k_B T$ barrier (see inset)). (b) Comparison between the velocity autocorrelation function of the original trajectories and of synthetic ones generated from the models using the Euler–Maruyama integrator. (c) Correlation analysis of the noise time series deduced from the trajectories in Fig. 3b by inverting the positional part of the VEC integrator.

testing the time-correlation of the noise inferred by interpreting the original MD trajectories as if they were generated by the Langevin models, compared with the expected analytical result (Fig. 4c). We note that here, i.e., in the case of MD simulation data, the interpretation of the noise correlation could be more subtle than for the benchmark one-dimensional system of Fig. 2, due to the long, non-exponential tail of the memory kernel. The probability density of the noise is well described by a standard Gaussian of zero mean and $2/3$ variance for different τ values, pointing again to reliable models, as shown in SI section C.

τ [ps]	MFPT [ns]
0.1	1.3 ± 0.1
0.2	1.6 ± 0.2
0.3	2.7 ± 0.3
0.4	2.8 ± 0.3
0.5	4.3 ± 0.4
1.0	2.3 ± 0.2
MD	3.6 ± 0.2

TABLE I. Mean first passage time (MFPT) for the different Langevin model, inferred using the likelihood correction, computed using Euler-Maruyama integrator, compared to the brute-force MFPT from all-atom MD simulations. Statistical uncertainties are estimated by block averaging.

An important motivation for the inference of stochastic models from limited, non-ergodic MD data is the attempt to predict kinetic properties without passing through cumbersome free-energy calculation techniques, often based on biased simulations^{32,33}.

We test the quantitative predictive power of the data-driven models of the fullerene dimer in water by comparing the predicted dissociation rate with the brute-force one: as shown in Table 1, the model with the best performance from the viewpoint of diagnostics ($\tau = 0.5$ ps) overestimates the MD rate by only 20%, whereas models with different τ have lower rates, but always in the same order of magnitude.

As shown in Fig. 4a, the model with the optimal τ (0.5 ps) but without likelihood correction yields a grossly inaccurate free-energy barrier ($\approx 30 k_B T$), consistent with the bad diagnostics in Fig. 4b,c. For other values of τ , the barrier is always overestimated and the rate cannot be reliably predicted.

Taken all together, these results demonstrate that the proposed correction to likelihood inference eliminates systematic errors originating from finite-difference CV velocity estimation: the new scheme is able to parametrize accurate underdamped Langevin models of real complex systems projected on a CV, even for barrier-crossing processes, despite of the use of short, non-ergodic trajectories. We underline the importance of the diagnostic tests we put forward to assess the pertinence and expected accuracy of the model in realistic scenarios, where the brute-force free-energy landscape or kinetic rate are not known beforehand.

The main limitation to the applicability of this method, being based on the Markovian Langevin equation, arises from the existence of long-time memory kernels in several realistic systems. To go beyond this hurdle, two possible strategies could be explored: i) increasing the dimensionality of the model to mitigate non-Markovian effects, or ii) adapting the approach developed in this work to the inference of generalized Langevin models, where memory effects are reproduced by the addition of hidden variables, based on expectation-maximization likelihood schemes³⁴.

III. ACKNOWLEDGEMENTS

This work was performed with the support of the Institut des Sciences du Calcul et des Données (ISCD) of Sorbonne University (IDEX SUPER 11-IDEX-0004). Calculations were performed on the GENCI-IDRIS French national supercomputing facility, under grant numbers A0110811069, A0130811069. We gratefully acknowledge Line Mouaffac and Jeremy Diharce for suggestions related to code development and simulations, as well as Pierre Ronceray for insightful discussions.

- ¹C. Moritz, A. Tröster, and C. Dellago, *The Journal of Chemical Physics* **147** (2017).
- ²P. Ditlevsen and S. Ditlevsen, *Nature Communications* **14**, 1 (2023).
- ³G. Milburn, *Contemporary Physics* **61**, 69 (2020).
- ⁴R. Zwanzig, *Nonequilibrium statistical mechanics* (Oxford University Press, 2001).
- ⁵E. Vanden-Eijnden and G. Ciccotti, *Chem. Phys. Lett.* **429**, 310 (2006).
- ⁶D. D. Girardier, H. Vroylandt, S. Bonella, and F. Pietrucci, *The Journal of Chemical Physics* **159**, 164111 (2023).
- ⁷G. Hummer, *New J. Phys.* **7**, 34 (2005).
- ⁸C. Micheletti, G. Bussi, and A. Laio, *J. Chem. Phys.* **129**, 074105 (2008).
- ⁹Q. Zhang, J. Brujić, and E. Vanden-Eijnden, *J. Stat. Phys.* **144**, 344 (2011).
- ¹⁰D. Crommelin and E. Vanden-Eijnden, *Multiscale Model. Simul.* **9**, 1588 (2011).
- ¹¹D. Crommelin, *Journal of Statistical Physics* **149**, 220 (2012).
- ¹²M. Baldovin, A. Puglisi, and A. Vulpiani, *PLoS One* **14**, e0212135 (2019).
- ¹³F. Sicard, V. Koskin, A. Annibale, and E. Rosta, *J. Chem. Theory Comput.* **17**, 2022 (2021).
- ¹⁴L. Donati, M. Weber, and B. G. Keller, *J. Math. Phys.* **63** (2022).
- ¹⁵K. Palacio-Rodriguez and F. Pietrucci, *J. Chem. Theory Comput.* **18**, 4639 (2022).
- ¹⁶D. B. Brückner, P. Ronceray, and C. P. Broedersz, *Phys. Rev. Lett.* **125**, 058103 (2020).
- ¹⁷N. Schaudinnus, B. Bastian, R. Hegger, and G. Stock, *Phys. Rev. Lett.* **115**, 050602 (2015).
- ¹⁸Moreover the equations of motion leading to the observed trajectory $q(t)$ are not of Langevin type (think to an experiment, or to high-dimensional MD projected on a CV), so that Eq. 1 is just a putative model of the original dynamics and it is meaningless to speak about.
- ¹⁹F. Ferretti, V. Chardes, T. Mora, A. M. Walczak, and I. Giardina, *Phys. Rev. X* **10**, 031018 (2020).
- ²⁰N. Schaudinnus, B. Lickert, M. Biswas, and G. Stock, *J. Chem. Phys.* **145**, 184114 (2016).
- ²¹B. Lickert, S. Wolf, and G. Stock, *The Journal of Physical Chemistry B* **125**, 8125 (2021).
- ²²H. Vroylandt, *EPL* **140**, 62003 (2022).
- ²³A. Jain, I.-H. Park, and N. Vaidehi, *J. Chem. Theory Comput.* **8**, 2581 (2012).
- ²⁴A. Drozdov and M. Morillo, *Phys. Rev. Lett.* **77**, 5324 (1996).
- ²⁵G. Bussi, D. Donadio, and M. Parrinello, *J. Chem. Phys.* **126**, 014101 (2007).
- ²⁶H. J. Berendsen, D. van der Spoel, and R. van Drunen, *Comput. Phys. Commun.* **91**, 43 (1995).
- ²⁷H. J. Berendsen, J. v. Postma, W. F. van Gunsteren, A. DiNola, and J. R. Haak, *J. Chem. Phys.* **81**, 3684 (1984).
- ²⁸W. L. Jorgensen, D. S. Maxwell, and J. Tirado-Rives, *J. Am. Chem. Soc.* **118**, 11225 (1996).
- ²⁹B. Peters, G. T. Beckham, and B. L. Trout, *J. Chem. Phys.* **127**, 034109 (2007).

³⁰L. Mouaffac, K. Palacio-Rodriguez, and F. Pietrucci, *J. Chem. Theory Comput.* **19**, 5701 (2023).

³¹H. Vroylandt and P. Monmarché, *J. Chem. Phys.* **156**, 244105 (2022).

³²F. Pietrucci, *Reviews in Physics* **2**, 32 (2017).

³³C. Chipot, *Annual Review of Biophysics* **52**, 113 (2023).

³⁴H. Vroylandt, L. Goudenège, P. Monmarché, F. Pietrucci, and B. Rotenberg, *Proc. Natl. Acad. Sci. U.S.A.* **119**, e2117586119 (2022).

Supporting Information:

Correcting systematic errors in the likelihood optimization of underdamped Langevin models of molecular dynamics trajectories

David Daniel Girardier,^{1, a)} Hadrien Vroylandt,² Sara Bonella,³ and Fabio Pietrucci¹

¹⁾*Sorbonne Université, Musée National d'Histoire Naturelle, UMR CNRS 7590, Institut de Minéralogie, de Physique des Matériaux et de Cosmochimie, IMPMC, F-75005 Paris, France*

²⁾*Université Caen Normandie, ENSICAEN, CNRS, Normandie Univ, GREYC UMR 6072, F-14000 Caen, France*

³⁾*Centre Européen de Calcul Atomique et Moléculaire (CECAM), Ecole Polytechnique Fédérale de Lausanne, Lausanne 1015, Switzerland*

(Dated: 23 June 2025)

^{a)}Electronic mail: david.girardier@sorbonne.universite.fr

A. Cumulants entering the propagator expression

We list here the cumulants obtained with the procedure from Ref.¹

$$\langle q \rangle = q_n + v_n \tau + \frac{1}{2}(\phi_n - \gamma v_n) \tau^2 \quad (\text{S1})$$

$$\langle v \rangle = v_n + (\phi_n - \gamma v_n) \tau - \frac{1}{2}[(\phi_n - \gamma v_n) \gamma - \phi_n^q v_n] \tau^2 \quad (\text{S2})$$

$$M_{qq} = \langle q^2 \rangle - \langle q \rangle \langle q \rangle = \frac{2}{3} c \tau^3 \quad (\text{S3})$$

$$M_{vv} = \langle v^2 \rangle - \langle v \rangle \langle v \rangle = 2c\tau - 2c\gamma\tau^2 + \frac{1}{3}(2c\phi_n^q + 4c\gamma^2)\tau^3 \quad (\text{S4})$$

$$M_{qv} = \langle qv \rangle - \langle q \rangle \langle v \rangle = c\tau^2 - c\gamma\tau^3 \quad (\text{S5})$$

with $c = k_B T \gamma / m$ and ϕ_n^q is the positional derivative of the force at q_n . The covariance matrix can then be written as

$$M = \begin{bmatrix} M_{qq} & M_{qv} \\ M_{qv} & M_{vv} \end{bmatrix} \quad (\text{S6})$$

B. Correspondence between the propagator and the integrator

In order to demonstrate the correspondence between our propagator derived from Ref.¹ and the VEC integrator², we write the propagator form of the integrator, in vector notation:

$$\begin{pmatrix} q_{n+1} \\ v_{n+1} \end{pmatrix} = \begin{pmatrix} q_n \\ v_n \end{pmatrix} + \begin{pmatrix} \tau - \frac{\gamma\tau^2}{2} \\ -\gamma\tau + \frac{\gamma^2\tau^2}{2} \end{pmatrix} v_n + \frac{\tau}{2} \begin{pmatrix} \phi_n \\ (1 - \gamma\tau)\phi_n + \phi_{n+1} \end{pmatrix} + \begin{pmatrix} \frac{\tau}{2\sqrt{3}}\sigma & \frac{\tau}{2}\sigma \\ -\frac{\gamma\tau}{2\sqrt{3}}\sigma & (1 - \frac{\gamma\tau}{2})\sigma \end{pmatrix} \begin{pmatrix} \tilde{G}_n \\ G_n \end{pmatrix} \quad (\text{S7})$$

Taking the average of this equation, we can identify the first moments $\langle q \rangle$, $\langle v \rangle$ and see that they are equivalent to our propagator if we assume that $\phi_n^q v_n \approx \frac{\phi_{n+1} - \phi_n}{\tau}$. We can compute the covariance matrix \tilde{M} as :

$$\tilde{M} = \begin{pmatrix} \frac{\tau}{2\sqrt{3}}\sigma & \frac{\tau}{2}\sigma \\ -\frac{\gamma\tau}{2\sqrt{3}}\sigma & (1 - \frac{\gamma\tau}{2})\sigma \end{pmatrix} \begin{pmatrix} \frac{\tau}{2\sqrt{3}}\sigma & \frac{\tau}{2}\sigma \\ -\frac{\gamma\tau}{2\sqrt{3}}\sigma & (1 - \frac{\gamma\tau}{2})\sigma \end{pmatrix}^T \quad (\text{S8})$$

with the following elements

$$\tilde{M}_{qq} = \frac{2}{3} c \tau^3 \quad (\text{S9})$$

$$\tilde{M}_{vv} = 2c\tau - 2c\gamma\tau^2 + \frac{2}{3}c\gamma^2\tau^3 \quad (\text{S10})$$

$$\tilde{M}_{qv} = c\tau^2 - \frac{2}{3}c\gamma\tau^3 \quad (\text{S11})$$

We can then see that they only differ at the order τ^3 in Eqs. S10, S11.

C. Finite-difference definition of velocities

Starting from the following definition of finite-difference velocities:

$$u_n^\lambda = (1 - \lambda)\frac{x_n - x_{n-1}}{\tau} + \lambda\frac{x_{n+1} - x_n}{\tau} \quad (\text{S12})$$

we can express the velocity for the VEC integrator as

$$u_n^\lambda = \left(1 - \frac{\gamma\tau}{2}\right) [\lambda v_n + (1 - \lambda)v_{n-1}] + \frac{\tau}{2} [\lambda F(x_n) + (1 - \lambda)F(x_{n-1})] \\ + \frac{\sigma}{2} \lambda [G_n + \frac{1}{\sqrt{3}}\tilde{G}_n] + \frac{\sigma}{2} (1 - \lambda) [G_{n-1} + \frac{1}{\sqrt{3}}\tilde{G}_{n-1}] \quad (\text{S13})$$

Using the update equation for the velocity, this leads to

$$u_n^\lambda = \left(1 - \frac{\gamma\tau}{2}\right) \frac{1 - \lambda \left(\gamma\tau - \frac{\gamma^2\tau^2}{2}\right)}{\alpha} v_n \\ + \frac{\tau}{2} \left[\lambda - \frac{(1 - \lambda) \left(1 - \frac{\gamma\tau}{2}\right)}{\alpha}\right] F(x_n) + \frac{\tau(1 - \lambda)}{2} \frac{\gamma\tau}{\alpha} F(x_{n-1}) \\ + \frac{\sigma}{2} \lambda [G_n + \frac{1}{\sqrt{3}}\tilde{G}_n] - \frac{\sigma(1 - \lambda)}{2} \frac{1 - \gamma\tau}{\alpha} G_{n-1} + \frac{\sigma(1 - \lambda)}{2} \frac{1}{\alpha} \frac{1}{\sqrt{3}} \tilde{G}_{n-1} \quad (\text{S14})$$

with

$$\alpha = \left(1 - \gamma\tau + \frac{\gamma^2\tau^2}{2}\right). \quad (\text{S15})$$

The Taylor expansion up to order τ gives

$$u_n^\lambda = (1 + \gamma\tau(1/2 - \lambda))v_n + \frac{\tau}{2}(2\lambda - 1)F(x_n) + \frac{\sigma}{2}\lambda[G_n + \frac{1}{\sqrt{3}}\tilde{G}_n] \\ - \frac{\sigma}{2}(1 - \lambda)G_{n-1} + \frac{\sigma}{2}(1 - \lambda)\frac{1 + \gamma\tau}{\sqrt{3}}\tilde{G}_{n-1} \quad (\text{S16})$$

Therefore, the difference is minimized for $\lambda = 1/2$.

$$u_n^{1/2} = v_n + \frac{\sigma}{4} \left[G_n + \frac{1}{\sqrt{3}}\tilde{G}_n - G_{n-1} + \frac{1}{\sqrt{3}}\tilde{G}_{n-1} \right] \quad (\text{S17})$$

Even though the derivation of this correction does not explicitly account for position-dependent friction. If we consider a case, where τ is small and $\gamma(q)$ do not vary drastically, it seems reasonable to allow the friction to be position dependent in the likelihood maximization.

D. Correlations of position, velocity and noise for the VEC integrator

$$\begin{aligned}
\langle v_n G_n \rangle &= 0 & \langle v_n \tilde{G}_n \rangle &= 0 \\
\langle v_n G_{n-1} \rangle &= \sigma - \gamma \frac{\tau}{2} \sigma & \langle v_n \tilde{G}_{n-1} \rangle &= -\gamma \frac{\tau}{2\sqrt{3}} \sigma \\
\langle v_n G_{n-2} \rangle &= \sigma - \gamma \frac{3\tau}{2} \sigma + \mathcal{O}(\tau^2) & \langle v_n \tilde{G}_{n-2} \rangle &= -\gamma \frac{\tau}{2\sqrt{3}} \sigma + \mathcal{O}(\tau^2)
\end{aligned}$$

$$\begin{aligned}
\langle x_n G_n \rangle &= 0 & \langle x_n \tilde{G}_n \rangle &= 0 \\
\langle x_n G_{n-1} \rangle &= \frac{\tau}{2} \sigma & \langle x_n \tilde{G}_{n-1} \rangle &= \frac{\tau}{2\sqrt{3}} \sigma \\
\langle x_n G_{n-2} \rangle &= \frac{3\tau}{2} \sigma + \mathcal{O}(\tau^2) & \langle x_n \tilde{G}_{n-2} \rangle &= \frac{\tau}{2\sqrt{3}} \sigma + \mathcal{O}(\tau^2)
\end{aligned}$$

E. Likelihood correction

In order to recover the properties of the integration velocity with respect to correlation in Eq. 7,8, we will need to rewrite the likelihood to express them. Going into this direction we first take minus the logarithm of the likelihood in Eq. 2.

$$\begin{aligned}
-\log \mathcal{L}_\theta &= \frac{1}{N} \sum \frac{1}{2} \ln(4\pi \det M) - \frac{1}{N} \sum \frac{M_{qq}}{2 \det M} (v' - M_v)^2 \\
&\quad - \frac{1}{N} \sum \frac{M_{vv}}{2 \det M} (q' - M_q)^2 + \frac{1}{N} \frac{M_{qv}}{\det M} \sum (v' - M_v)(q' - M_q)
\end{aligned} \tag{S18}$$

We can take variances (Eq. S3, S4, S5) out of the sums in Eq. S18 to express it as

$$\begin{aligned}
-\log \mathcal{L}_\theta &= \frac{1}{N} \sum \frac{1}{2} \ln(4\pi \det M) - \frac{M_{qq}}{2 \det M} \langle (v' - M_v)^2 \rangle \\
&\quad - \frac{M_{vv}}{2 \det M} \langle (q' - M_q)^2 \rangle + \frac{M_{qv}}{\det M} \langle (v' - M_v)(q' - M_q) \rangle
\end{aligned} \tag{S19}$$

with

$$\begin{aligned}
\langle (q' - M_q)^2 \rangle = & \langle q'^2 \rangle + \langle q^2 \rangle - 2\langle qq' \rangle + \langle vq' \rangle(-2\tau + \gamma\tau^2) + \langle vq \rangle(2\tau - \gamma\tau^2) \\
& + \langle v^2 \rangle(\tau^2 - \gamma\tau^3 + \frac{1}{4}\gamma^2\tau^4) - \langle \phi q' \rangle\tau^2 + \langle \phi q \rangle\tau^2 \\
& + \langle \phi v \rangle(\tau^3 - \frac{1}{2}\gamma\tau^4) + \frac{1}{4}\langle \phi^2 \rangle\tau^4
\end{aligned} \tag{S20}$$

$$\begin{aligned}
\langle (v' - M_v)^2 \rangle = & \langle v'^2 \rangle + \langle v'v \rangle(-2 + 2\gamma\tau - \gamma^2\tau^2) \\
& + \langle v^2 \rangle(1 - 2\gamma\tau + 2\gamma^2\tau^2 - \gamma^3\tau^3 + \frac{1}{4}\gamma^4\tau^4) + \langle \phi v' \rangle(-2 + \gamma\tau^2) \\
& + \langle \phi v \rangle(2 - 3\gamma\tau^2 + 2\gamma^2\tau^3 - \frac{1}{2}\gamma^3\tau^4) + \langle \phi^2 \rangle(\tau^2 - \gamma\tau^3 + \frac{1}{4}\gamma^2\tau^4) \\
& - \langle vv'\phi_q \rangle\tau^2 + \langle v^2\phi_q \rangle\tau^2 + \langle v\phi\phi_q \rangle\tau^3 - \langle v\phi_q \rangle\gamma\tau^3 - \frac{1}{2}\langle v\phi\phi_q \rangle\gamma\tau^4 \\
& + \frac{1}{2}\langle v^2\phi_q \rangle\gamma^2\tau^4 + \frac{1}{4}\langle v^2\phi_q^2 \rangle\tau^4
\end{aligned} \tag{S21}$$

$$\begin{aligned}
\langle (q' - M_q)(v' - M_v) \rangle = & \langle v'q' \rangle - \langle v'q \rangle \\
& + \langle vq' \rangle(-1 + \gamma\tau - \frac{1}{2}\gamma^2\tau^2) + \langle vq \rangle(1 - \gamma\tau + \frac{1}{2}\gamma^2\tau^2) \\
& + \langle vv' \rangle(-\tau + \frac{1}{2}\gamma\tau^2) + \langle v^2 \rangle(\tau - \frac{3}{2}\gamma\tau^2 + \gamma^2\tau^3 - \frac{1}{4}\gamma^3\tau^4) \\
& + \langle \phi q' \rangle(-\tau + \frac{1}{2}\gamma\tau^2) + \langle \phi q \rangle(\tau - \frac{1}{2}\gamma\tau^2) \\
& - \frac{1}{2}\langle \phi v' \rangle + \langle \phi v \rangle(\frac{3}{2}\tau^2 - \frac{3}{2}\gamma\tau^3 + \frac{1}{2}\gamma^2\tau^4) + \langle \phi^2 \rangle(\frac{1}{2}\tau^3 - \frac{1}{4}\gamma\tau^4) \\
& - \frac{1}{2}\langle vq'\phi_q \rangle\tau^2 + \frac{1}{2}\langle vq\phi_q \rangle\tau^2 + \frac{1}{2}\langle v^2\phi_q \rangle\tau^3 \\
& + \frac{1}{4}\langle v\phi\phi_q \rangle\tau^4 - \frac{1}{4}\langle v^2\phi_q \rangle\gamma\tau^4
\end{aligned} \tag{S22}$$

Now that the correlations of Eq. 7,8 appear in the previous expressions it is then possible to account for the use of finite difference velocities.

F. Generalized Langevin equation

Any high-dimensional Hamiltonian system projected onto one (or few) CV at a fine time resolution can be described by a generalized Langevin equation of the following form

$$\begin{cases} \dot{q} = v \\ \dot{v} = -\frac{1}{m}dF/dq - \int_0^t dt' K(t')v(t-t') + R(t) \end{cases} \quad (\text{S23})$$

where m is an effective mass (see below), $F(q) = -k_bT \log \rho_{eq}(q)$ is the free energy profile (potential of mean force) corresponding to the equilibrium density, $K(t)$ is a history-dependent friction kernel, and $R(t)$ is a random force (noise), related to friction via the fluctuation-dissipation theorem^{3,4}.

G. Noise Analysis

We also propose a way to validate the accuracy of the inference. This can be achieved by analyzing the noise that would have been required to reproduce the initial trajectories using the optimal Langevin model. In the absence of the issues arising from finite-difference velocities, the recovered noise should be centered around zero, exhibit unit variance, and be delta-correlated in time. To analyze this, we focus on the positional part of the numerical integrator (Eq. 4), combining the two noise terms and isolating them as:

$$\mathcal{G}_n = G_n + \frac{1}{\sqrt{3}}\tilde{G}_n = \left(\frac{q_{n+1} - q_n}{\tau} - \left(1 - \frac{\gamma\tau}{2}\right)v_n - \frac{\tau}{2}\phi_n \right) \frac{2}{\sigma} \quad (\text{S24})$$

Using properties of Gaussian white noises and Eq. 7,8, it is possible to obtain the following properties of \mathcal{G}_n :

$$\langle \mathcal{G}_n \rangle = 0, \quad \langle \mathcal{G}_n^2 \rangle = \frac{2}{3}, \quad \frac{\langle \mathcal{G}_n \mathcal{G}_{n+1} \rangle}{\langle \mathcal{G}_n^2 \rangle} = \frac{1}{4} \quad (\text{S25})$$

H. unmodified fullerenes dimer in water

We present here the free energy profiles, for the underdamped models trained on fullerenes dimer in water projected onto the distance between the two centers of mass. The masses of the carbon and oxygen are unmodified, in order to show that the system does not display an underdamped regime.

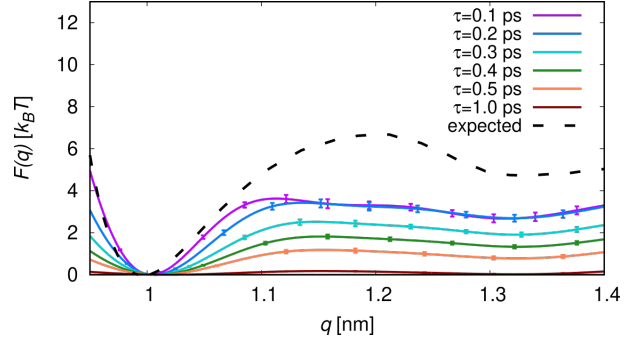


FIG. 1. Free-energy profiles at different time resolutions τ using the likelihood correction, for unmodified masses system.

REFERENCES

- ¹A. N. Drozdov, Phys. Rev. E **55**, 2496 (1997).
- ²E. Vanden-Eijnden and G. Ciccotti, Chem. Phys. Lett. **429**, 310 (2006).
- ³R. Kubo, Rep. Prog. Phys. **29**, 255 (1966).
- ⁴H. Vroylandt, EPL **140**, 62003 (2022).